



Electrochemical Migration Behavior on FR-4 Printed Circuit Board with Different Surface Finishes

Xiaoxiao Song¹ · Keyu Wang¹ · Zhuo Chen² · Kaixu Ren³ · Peng Liu³

Received: 26 February 2023 / Accepted: 12 June 2023 / Published online: 30 June 2023
© The Minerals, Metals & Materials Society 2023

Abstract

The impact of four typical surface finishes on electrochemical migration in printed circuit board production was studied using a modified water drop test, and the electrochemical migration phenomena of each surface finish at different bias voltages were analyzed. Based on the analysis of the experimental results, the four surface finishes were ranked in terms of their ability to resist electrochemical migration, as follows: electroless nickel/immersion gold (ENIG) > lead-free hot air solder leveling (HASL) > HASL > Cu. For the lead-free HASL, HASL, and Cu surface finishes, the growth of dendrites was mainly related to the hydroxide solubility product of metal ions, with a smaller solubility product leading to a larger area of precipitates, which further hindered the emergence and growth of dendrites. The electrochemical migration process of ENIG differed from other surface finishes. Gold was not involved in the electrochemical migration process, and no typical cathodic dendrite growth phenomenon was observed. Only nickel hydroxide and oxide formed from the anode edge and migrated toward the cathode with low conductivity, resulting in high electrochemical migration resistance for the ENIG surface finish.

Keywords Electrochemical migration (ECM) · surface finish · printed circuit board (PCB) · dendrite growth

Introduction

With the trend toward smaller and lighter electronic devices, the significant reduction in component size has led to tighter packaging of components on printed circuit boards (PCB), resulting in the interconnection of various circuits and the simultaneous use of multiple materials. The spacings associated with some surface mount technology (SMT) circuits are reduced to a minimum of 0.1 mm.¹ The drawback of these technological advances is that electronic devices are increasingly susceptible to failure, especially failure due to corrosion.^{2,3}

As one of the main corrosion failure modes, electrochemical migration (ECM) can cause insulation resistance degradation and short circuits. With the trend of small pitch

distance and spacing between conductors, ECM is frequently observed and can cause serious failure issues.⁴

Dendrite growth in ECM consists of three main stages: anodic dissolution, ion diffusion migration, and cathodic deposition. The phenomenon can be specifically described as two electrodes with voltage bias that are close together and connected by a thin film of adsorbed liquid or condensed water droplets under wet conditions. Metal ions will dissolve from the anode and migrate to the cathode to form dendritic crystals. Dendrites grow between the electrodes and eventually establish a connection leading to a sudden spike in current, which further facilitates dendrite growth. The dendrites continue to grow and eventually lead to the failure of the component. With the tendency toward spacing reduction between conductors, ECM is frequently observed between exposed pads on PCBs or within packages, which causes serious failure problems.^{5–7}

In the PCB manufacturing industry, metallic surface finishing of the exposed electrodes on the PCB is critical for improving reliability, conductivity, and solderability. The sensitivity of different PCB electrode surface finishes to ECM varies widely. Several studies have been conducted to analyze the ECM phenomenon with common metallic materials on PCBs, including pure tin,^{2,8} tin-based solder

✉ Xiaoxiao Song
xxsong@cauc.edu.cn

¹ Sino-European Institute of Aviation Engineering, Civil Aviation University of China, Tianjin 300300, China

² Institute of Aviation Engineering, Civil Aviation University of China, Tianjin 300300, China

³ China Automotive Technology and Research Center Co., Ltd., Tianjin 300162, China

alloys,^{1,9,10} and sintered nano-silver.^{11,12} Similarly, some of the studies were based on different surface finishes of PCBs, including hot air solder leveling (HASL),¹³ immersion silver (ImAg),^{14,15} copper-clad laminate (Cu),¹⁶ and electroless nickel/immersion gold (ENIG).^{17,18}

Noh et al.¹⁹ conducted water drop (WD) experiments for Cu, and ENIG surface finishes and found that the main elements forming dendrites were copper, nickel, and gold, respectively, and that ENIG was the most resistant to the occurrence of ECM. In addition, the mechanisms of ECM occurring in different surface finishes are different, where the main component of dendrites generated by ENIG is gold. He et al.¹ conducted a temperature-humidity-bias (THB) test using standard comb circuit boards to investigate the current leakage and ECM behavior on HASL PCBs, and found that tin was the main migrating metal and was observed as either a layer or in polyhedral deposits. The main component of the dendrites was lead, and only a small fraction of the migrated metal was copper. Hong et al.²⁰ conducted THB exposure tests on FR-4 PCBs with four different surface finishes, and the results yielded a ranking of ECM sensitivity for different surface finishes and electrode pitch, where for the same pitch, the mean time to failure of copper is shorter than that of the HASL. The accelerated lifetime prediction of ECM was further obtained from ENIG experimental data. Bušek et al.²¹ conducted extensive water drop experiments on test boards with different surface finishes at constant voltage and concluded that ENIG is more resistant to ECM and that the surface finish has no direct effect on dendrites, but rather on the compounds formed between the surface finish and the solder. Medgyes et al.²² performed water drop experiments through comb boards with copper, immersion tin, immersion silver, and tin-lead alloy HASL surface finishes. The results showed that the respective ECM rates of the different metals were, from largest to smallest: Ag, Cu, and Sn, but the relationship between Pb and Cu could not be determined. The comparison of pure metal and solder alloy surface treatments leads to uncertain mean time to failure results, probably due to the formation of eutectic solid solutions and

the flux content in the solder alloy, causing the difference in solubility constants of the ions, which can significantly affect the ECM behavior of copper. Illés et al.²³ conducted a comparative study of the ECM behavior of three different surface finishes—copper, immersion tin, and immersion silver—under vapor phase soldering (VPS) and infrared reflow (IR). It was concluded that the VPS process did not change the reliability of the microelectronic components and the rate of ECM for the three surface finishes was, from largest to smallest: immersion silver, copper, and immersion tin. Therefore, the ECM sensitivity ranking and ECM products of the surface finishes derived from each study are not the same, and further analysis of the ECM process and its mechanism for regular surface finishes is required.

The impact of four typical surface finishes applied in PCB production on ECM was investigated using a modified water drop method, with in situ observation and current monitoring between electrodes for each surface finish under different bias voltages. The ECM experimental results were further investigated by product morphology and composition analysis tests to study the ECM behavior of different surface finishes. The ECM rate, product composition, and ECM resistance of the test boards were further discussed.

Experimental and Methods

Material

The substrate material of the PCB test board is FR-4 glass fiber resin, with pure copper electrodes and trace micro-etched on the FR-4 substrate. The test boards are covered with solder mask in areas other than the copper electrodes, where the surface finishes are applied: on the exposed pure copper electrodes. Apart from the ones without further surface finishing (bare Cu), the remaining three surface finishes are completed by tin spraying or chemical plating based on the copper electrode surface. The structure of different surface finishes is shown as Fig. 1a

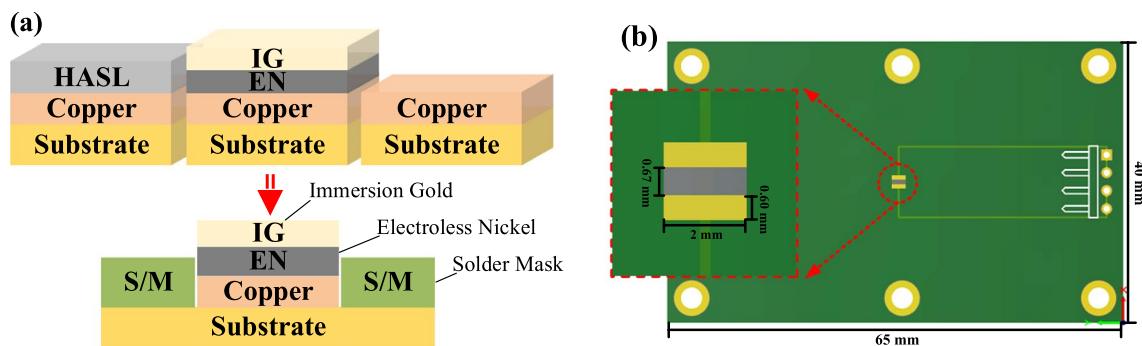


Fig. 1 Schematic of (a) surface finishes structure, (b) test board configuration.

Based on the design of the small outline integrated circuit (SOIC) footprint according to IPC-7351B, with the standard form of flat rectangular pads, the test patterns with different surface finishes are designed to perform a modified water drop test in order to simulate the ECM process between adjacent pads of the footprint. Specifically, as is shown in the Fig. 1b, the designed PCB is 65 (L) × 40 (W) × 1.6 (T) mm, the two electrodes on the board are both 0.60 mm × 2 mm, and the electrode spacing is 0.67 mm. Apart from the exposed electrodes and the space between them, the rest of the FR-4 substrate is also covered by solder mask to avoid the influence of water droplets and other contaminants on the experiment.

Experimental Setup

As shown in Fig. 1a, after ultrasonic treatment in acetone solution and hot air drying, the test board is bonded with a droplet limit board with a thickness of 1 mm by a double-sided hot melt adhesive film. In the center of the droplet limit board, a circular hole with a radius of 1.5 mm is drilled at the test pattern position to ensure the droplet covers the test pattern. A modified water drop test device was built as shown as Fig. 2b. To enable in situ observation of the ECM process, a microscope was installed above the test board. A four-pin header was soldered to the through holes on the bonded test board, which is connected to the electrical connection between the test patterns and the electrochemical workstation electrodes, namely the sense electrode (SE), working electrode (WE), counter electrode (CE) and reference electrode (RE). In the circuit, the sense electrode and the working electrode are connected to the anode on the PCB, and the counter electrode and the reference electrode are connected to the cathode. Therefore, the instrument can apply different magnitudes of voltage bias between the PCB test pattern. This modified water drop method can efficiently control the volume and shape of the liquid film covering the electrodes, and reduce reflections in the microscopic

observation process while avoiding the formation of dendrites at the edge of the droplet due to uneven mass transfer.

During the experiment, a droplet of 5 μL deionized water was injected into the circular hole at ambient temperature ($\sim 25\text{ }^\circ\text{C}$), which covers the test pattern. The required potential was applied between the electrodes using the potentiostatic polarization mode on a PARSTAT 2273 instrument. The current between the electrodes was measured and recorded continuously throughout the experiment. At the same time, the in situ microscopic observation and recording were achieved by a ZEISS Stemi 508 microscope. A scanning electron microscope (Hitachi S-3400) was used to observe the morphology of the ECM products and surface of the test board. Elemental analysis was performed using the accompanying energy-dispersive spectroscopy (EDS).

Results and Discussion

Time-Dependent Surface Evolution and Failure Analysis

ECM experiments were performed on lead-free HASL, HASL, Cu, and ENIG finishing under four sets of voltage bias at 3 V, 5 V, 8 V, and 10 V. The experimental results are shown in Fig. 3.

Since the reaction was not apparent in some experimental groups under 3 V bias, and the reaction process was too quick to observe the phenomenon under higher voltage bias, the in situ images of the ECM process were collected under 5 V bias (the phenomenon was not obvious under low voltage for the ENIG group, which is why the bias voltage was selected as 10 V in the figure). Throughout the experiment, bubbles were continuously emerging at the cathode and anode edges, and the number and size of bubbles were much greater at the cathode than at the anode. ECM products with different morphologies appeared between the electrodes with increasing time in each experimental group. In both the

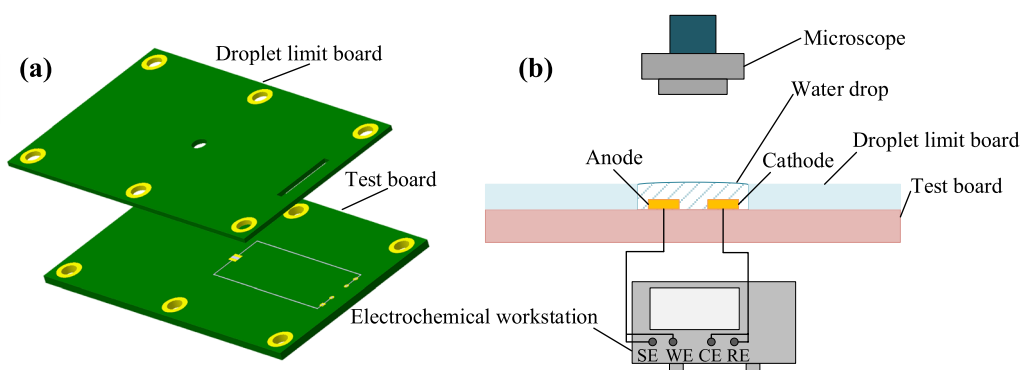


Fig. 2 Schematic of (a) droplet limit board installation, (b) water drop experimental setup.

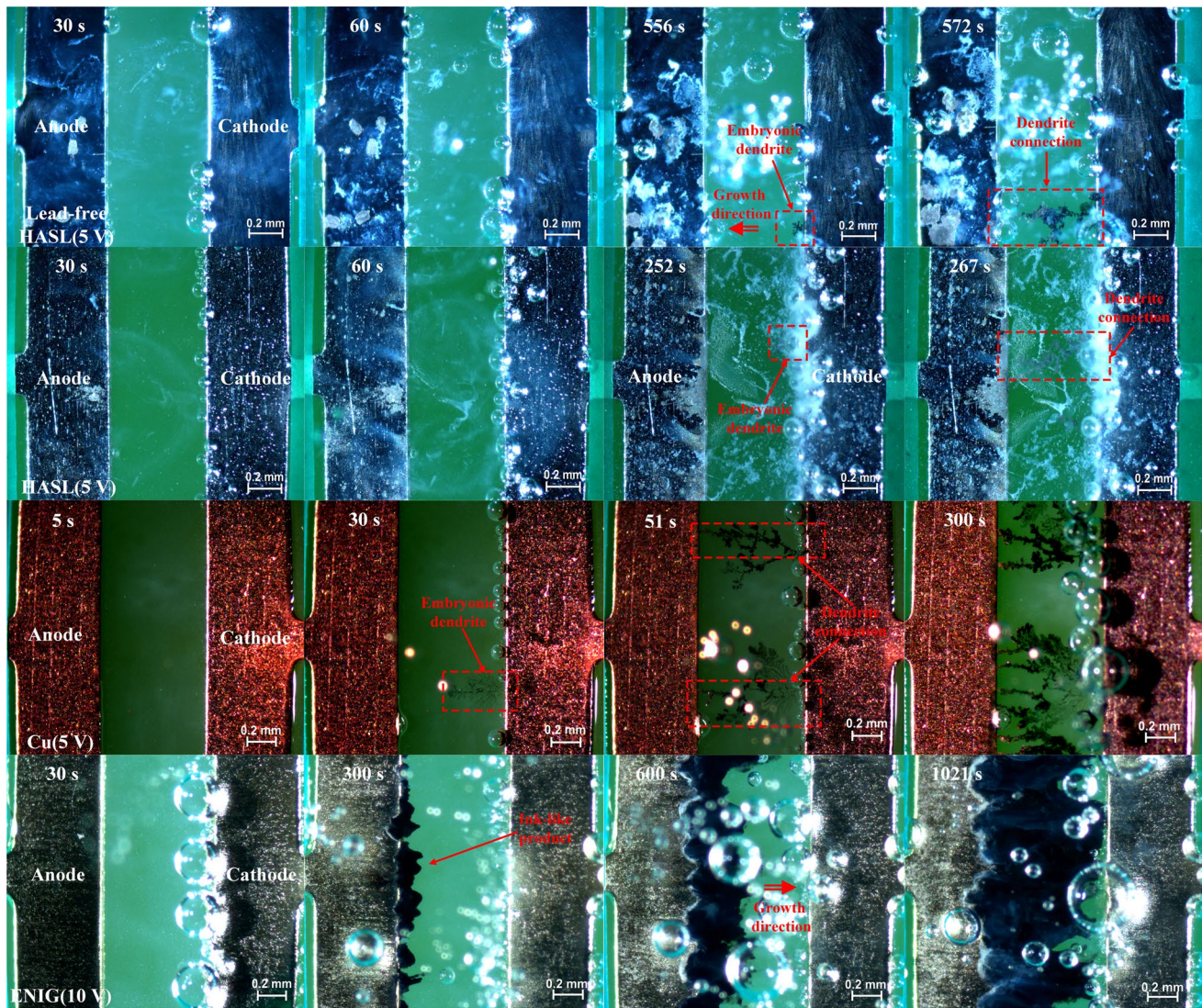


Fig. 3 In situ microscope photos of different surface finishes under 5 V bias voltage (10 V for ENIG).

lead-free HASL and tin-lead HASL experimental groups, white precipitates appeared in the solution and accumulated between the electrodes as the reaction proceeded. Except for the ENIG group, embryonic dendrites (the dark protrusion marked in red, darker gray for the HASL group) emerged at the edge of the cathode, which later crept toward the anode and, at the late stage of the experiment, touched the edge of the anode (corresponding to lead-free HASL 572 s; HASL 267 s; Cu 51 s in Fig. 3). In the meantime, a surge of current was found on the real-time current curve in Fig. 4, implying a local short-circuit phenomenon occurred at this location. Moreover, for the ENIG group, uniform black precipitation at the anode was observed during the experiment. This product kept spreading toward the cathode between the electrodes, and was shaped more uniformly and developed at a slower rate compared to the dendrite growth from the other

groups, which barely reached the opposite electrode at all applied bias voltages.

Further analysis of the current variation showed a similar trend in the early stages of experiments under different voltage bias, the numerical magnitude of the current increases as the bias voltage rises, which can be explained by the high dissolution rate of the anode metal at relatively high applied voltages and the faster ion migration under the influence of higher field strengths and therefore higher current density. However, for the first three surface finishes, the currents did not stabilize with time, but showed a steep increase in current, and microscopic short circuits were observed at different time points, which corresponded to the first dendrite connection time in Fig. 3. This indicates that the dendrite connection would directly cause a sharp increase in the current and lead to microscopic short circuits. After the first

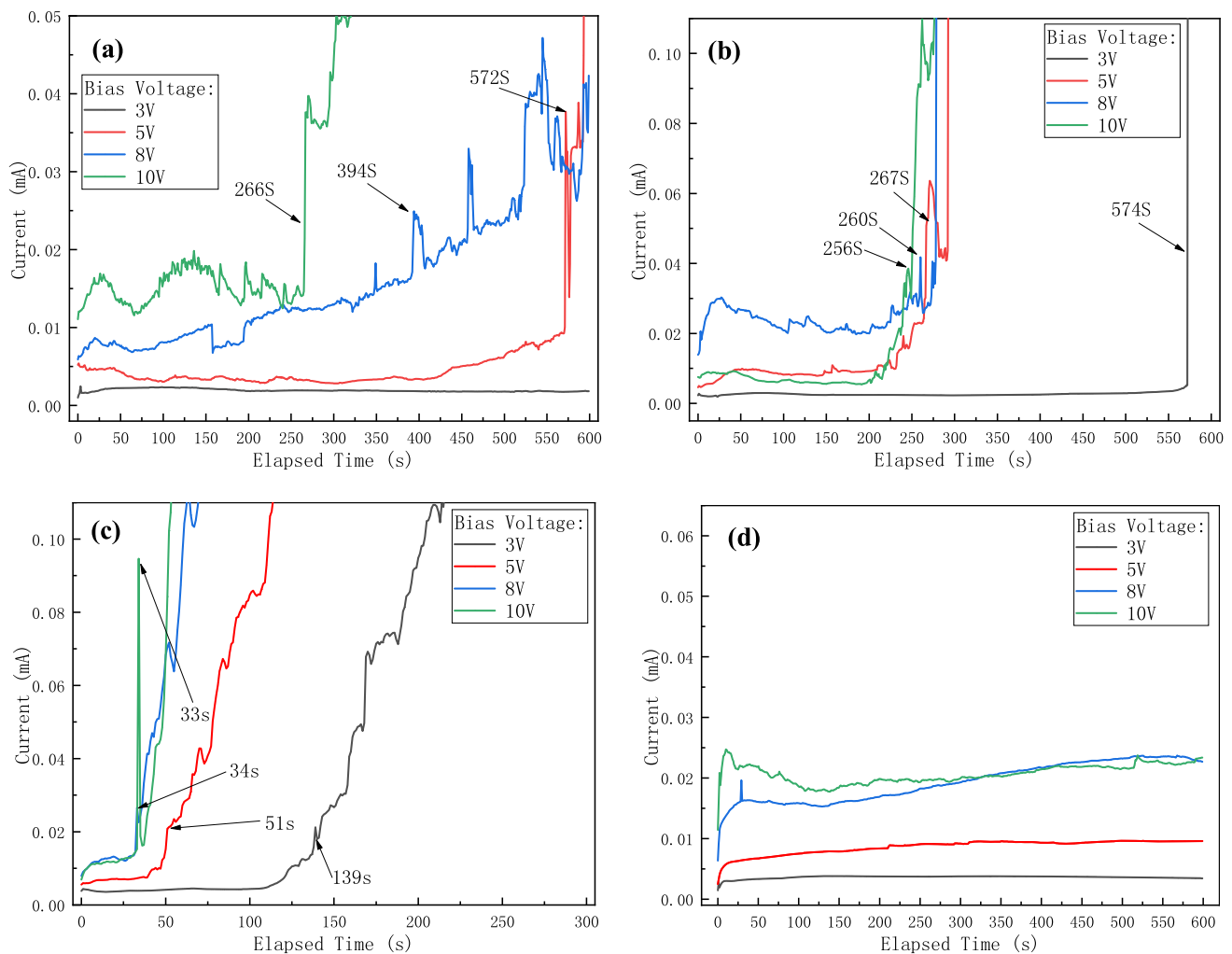


Fig. 4 Current-time curves of samples under different bias voltages: (a) lead-free HASL, (b) HASL, (c) Cu, (d) ENIG.

dendrite connection occurred on the test board, the current continued to fluctuate abruptly, indicating that the dendrites continued to connect and disconnect the electrodes, at which point the surface insulation resistance of the test board has fallen into the failure zone. It is worth noting that the short-circuit current of the Cu test board after the failure of the dendrite continuity is extremely high, reaching a maximum of 15 mA at 10 V (not shown in Fig. 4 due to scale limitation). This value is much higher than the results of the HASL test board. At the same time, it can be seen from Fig. 4 that the time to failure for the Cu test board at all voltages is very small, while the current keeps surging after the first failure (dendrite connection), which also indicates that the number of dendrites connected in this experimental group is very large and that the fracture of some connected dendrites does not have a great impact on the short-circuit current.

The electrode spacing, temperature, external contamination, and bias voltage all have significant effects on the time to failure, which is the most intuitive way to characterize

ECM.²⁴ The time to failure (TTF) was counted for each group of experiments, which was defined as the time when the dendrite connection first occurred on the test board. The TTF for test boards without failure was assigned with the maximum experimental duration of 900 s. The box diagram was as shown in Fig. 5 (no corresponding box diagram for ENIG since the failure did not occur).

In Fig. 5, it can be seen that, for different surface finishes, from 3 V to 10 V, the test board failure time decreases significantly with increasing voltage. Fig. 5a shows that the lead-free HASL did not fail for all test boards at 3 V. Starting from 5 V, the failure mainly occurs between 300 s and 800 s, while there are still some specimens that do not fail at 5 V and 8 V, indicating that the lead-free HASL surface finish has some resistance to ECM. Comparing Fig. 5a and b, it can be seen that the failure time of HASL test boards is much lower than that of lead-free HASL test boards, and that the majority of HASL test boards fail within 100–300 s under 5 V or higher bias voltages. As seen in Fig. 5c, the

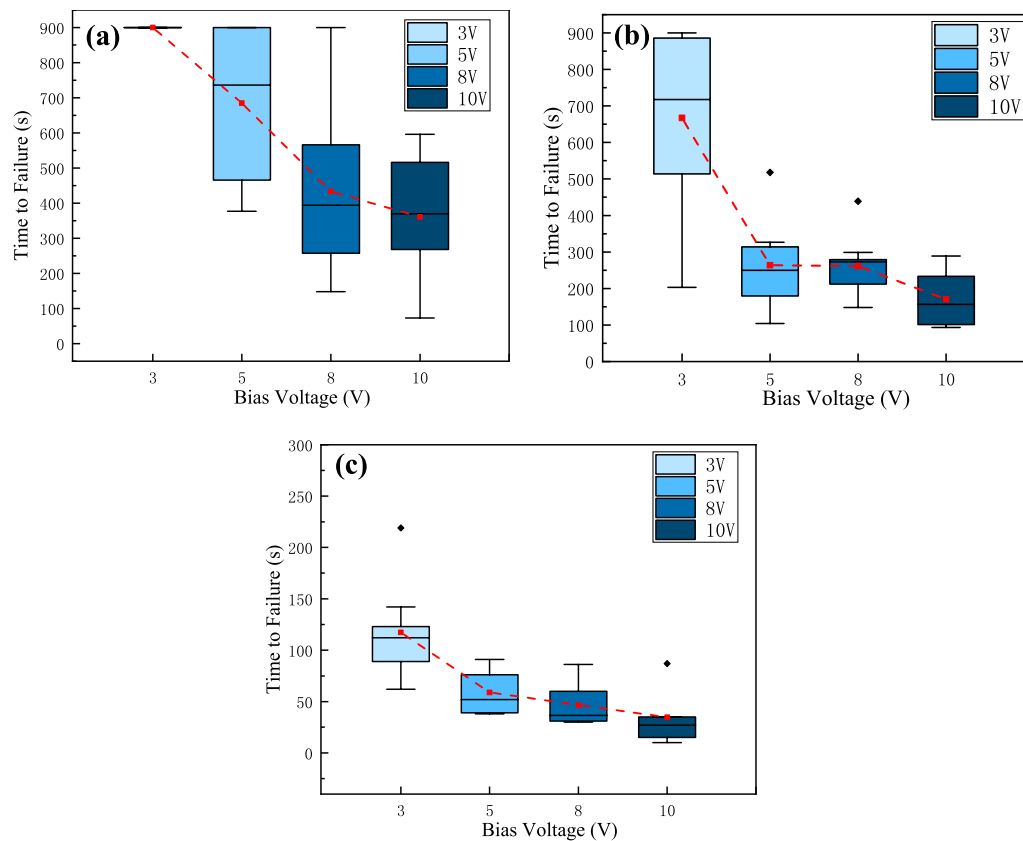


Fig. 5 Box diagram of failure of samples with different surface finishes under different bias voltages: (a) lead-free HASL, (b) HASL, (c) Cu.

failure time of the Cu test boards is much lower than that of HASL and lead-free HASL. Under all bias voltage conditions, the Cu test boards fail within 150 s, and the failure time decreases as the voltage increases.

Morphology and Microstructure of ECM Products

In order to carry out the observation and comparison of the morphology for different surface finishes after the experiment, the corresponding ECM product morphologies for each surface finish were further studied, with the microscopic surface morphology between the electrodes shown in Fig. 6.

As shown in Fig. 6a, for the lead-free HASL test board, ECM products are present in some locations on the substrate between the electrodes. There are two main morphologies. One is a porous, gully-like dendrite I, and the other is the typical tree-branch dendrite II. The superposition of these two types of dendrites is visible between the electrodes. As shown in Fig. 6b, the ECM products appearing between the electrodes of the HASL test board demonstrate a typical dendritic structure, which can be further seen in the magnified view during the growth from the cathode to the anode. The dendrites are not entirely fractal in the position close to

the anode, while the dendrites far from the anode are fully formed with thin branches. As shown in Fig. 6c, the ECM product morphology of the Cu test board is different from the former two surface finishes in that there is no apparent dendritic structure, but a cluster-like aggregation, similar to the type I dendrite morphology in lead-free HASL. At the same time, the overall image still shows a branching structure. The cathode of the Cu test board shows a large number of bumps with rough edges, and the uneven electric field distribution caused by these bumps is one of the reasons for triggering dendrite growth. Finally, as shown in Fig. 6d, many scale-like products were found on the surface of the ENIG test board after the experiment. Compared with the image of the ENIG test board, after 900 s in Fig. 3, it can be observed that the black–green products were dehydrated and broken up due to the complete evaporation of the liquid droplets after the experiment, and black scale-like products were dispersed between the electrodes.

The ECM products from different surface finishes were further studied by EDS composition analysis, and the results are shown in Table I (the positions of EDS analysis are shown in Fig. 6).

It can be seen that the metal elements in the ECM products of lead-free HASL in deionized water are mainly Cu

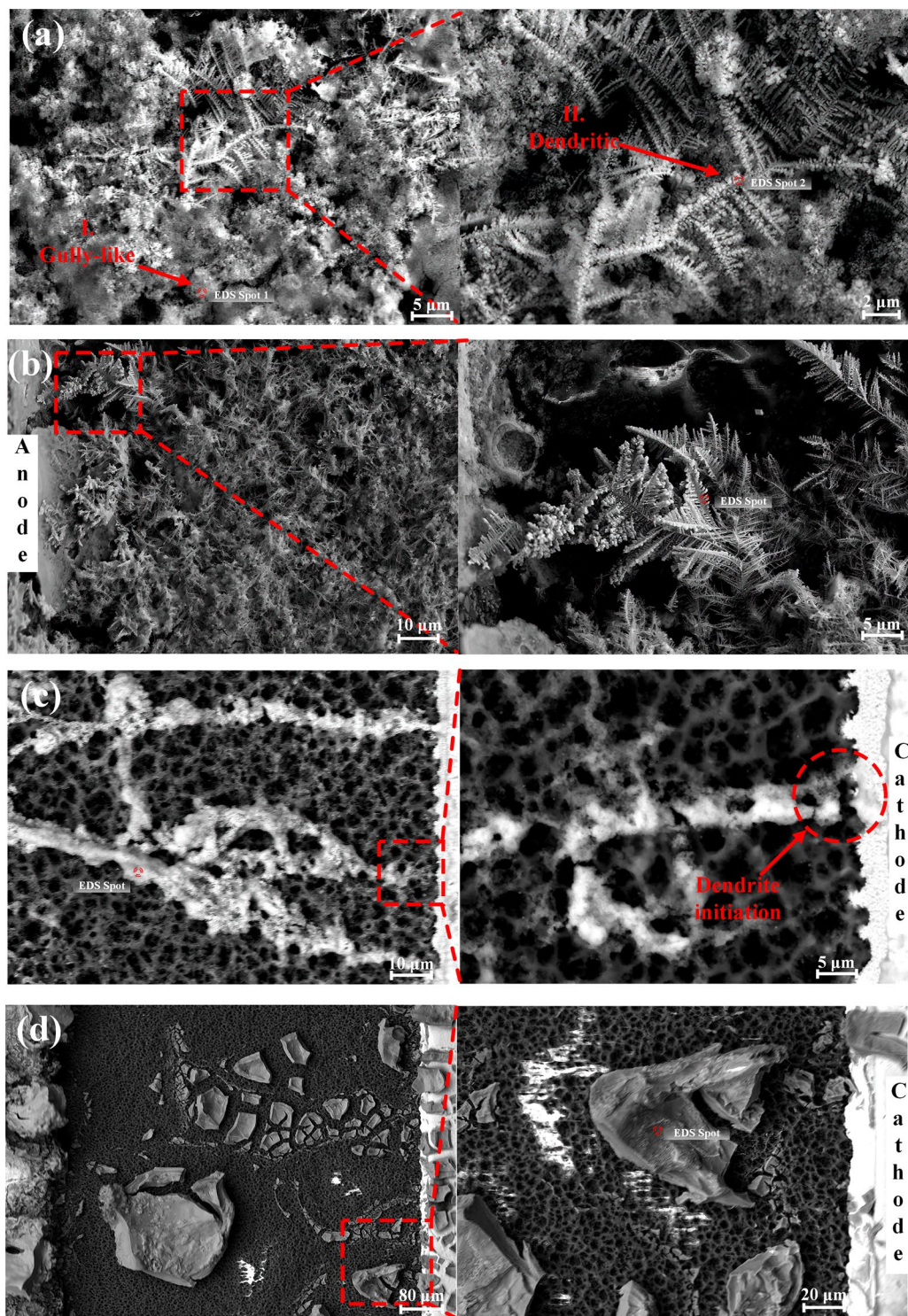


Fig. 6 Typical dendrites morphology of (a) lead-free HASL, (b) HASL, (c) Cu, (d) ENIG.

and Sn. The rest are very small amounts of Al from the substrate and also Pb. The presence of Cu is mainly due to the peeling of the lead-free HASL surface finish during the dissolution of the anode, resulting in the exposure and dissolution of the bottom copper layer. In addition, the existence

of pores on the surface of the lead-free HASL allows the solution to penetrate the interior of the anode resulting in the dissolution of Cu. As shown in Table I, there is a huge difference in the composition of the two morphological dendrites of lead-free HASL, with Cu being the highest in the

composition of the gully-shaped dendrite I, accounting for 77.64 wt.%, while the main component of the dendrite II is the element Sn, accounting for 73.55 wt.%. Therefore, it is inferred that the main reason for the formation of the tree-branch dendrites is the high content of Sn.

The compositional analysis of the HASL surface finish revealed that the main components of the dendrites are Sn and Pb, with the mass fraction of Sn being higher than that of Pb. The composition of the dendrites shows that Sn dominated the dendrites from the HASL surface finish, while Pb is one of the main components of the dendrites after Sn in terms of mass fraction.

The main components of the dendrites for the Cu surface finish are Cu and O, where the content of Cu is close to 95 wt.%, which proves that the products of ECM are mainly composed of Cu metal.

The main components of the black substance for the ENIG surface finish are Ni and O (as shown in Fig. 7 and

Table I), which indicates that the main migrated metal is Ni. Also, Au is not observed from the elemental analysis and surface scan results, indicating that Au is not involved in the ion migration process.

ECM Conditions for Different Surface Finishes

For each surface finish, the application of bias voltage between the electrodes results in the dissolution of different metal anodes to produce a large number of metal ions, and the process is influenced by their standard electrode potentials, while the maximum metal ion concentration within the solution is controlled by the formation of hydroxide precipitation, so the difficulty for dendritic deposition to appear is determined by both the standard electrode potential of the metal and the solubility of the corresponding hydroxides. Therefore, the process of ECM was further analyzed by the

Table I Elemental composition of products with different morphologies (weight %)

Element/surface finish	Cu	Sn	C	O	Al	Ni	P	Pb
Lead-free HASL I	77.64	4.26	10.90	7.20	–	–	–	–
Lead-free HASL II	3.65	73.55	12.33	9.70	1.89	–	–	0.28
HASL	–	76.48	–	–	0.97	–	–	22.55
Cu	94.63	–	–	5.37	–	–	–	–
ENIG	–	–	–	37.23	–	60.85	1.92	–

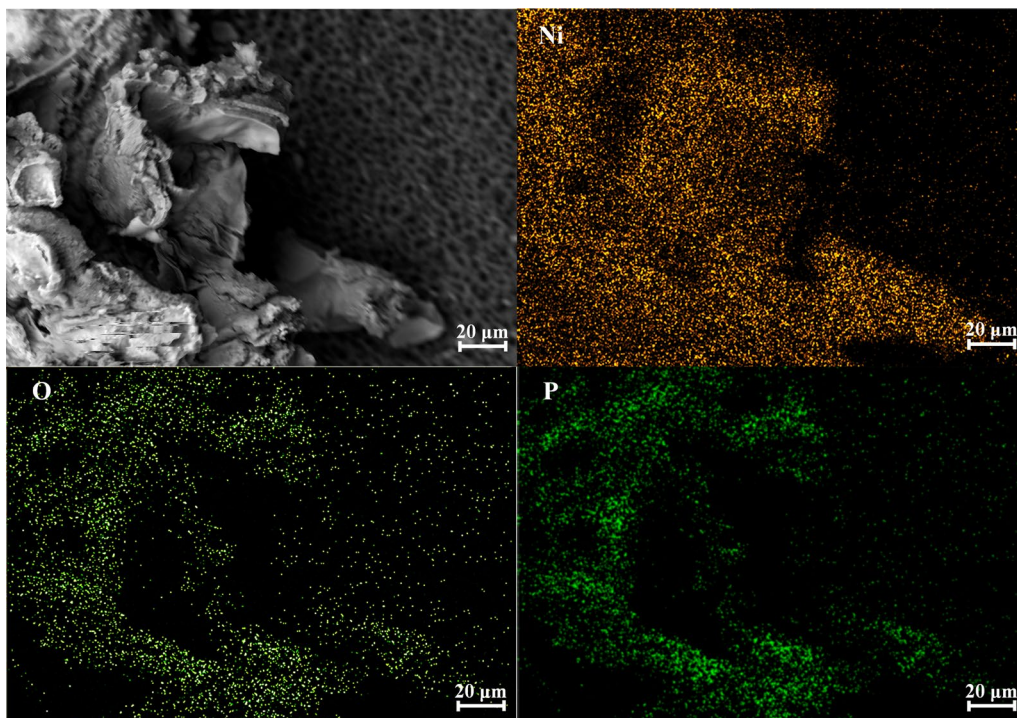


Fig. 7 Surface scan of the substance between the ENIG electrodes.

hydroxide properties and standard electrode potentials of the metals involved in each surface finish.

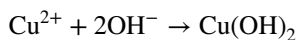
Furthermore, an in situ observation was performed by applying a 3 V bias voltage to the test board with lead-free HASL surface finish by adding agar with universal pH indicator replacing the water droplet as the ECM medium. As shown in Fig. 8, a large amount of white precipitates appeared between the electrodes at the beginning of the experiment in the first 300 s. The surface of the anode electrode showed a yellow color and the surface of the cathode showed a blue color. The blue color near the cathode indicates that a large amount of OH^- generated at the cathode diffuses along the concentration gradient toward the anode, which encounters metal ions dissolved from the anode, and in turn continuously produces hydroxides between the electrodes. Due to the low solubility of the tin hydroxide, a large precipitate forms when the tin ion and the OH^- ion meet, and a large region of precipitation appears. When the metal ions try to migrate through the precipitation region to the cathode, they are intercepted by the OH^- ions and form new areas of precipitation every time they meet, so a precipitate wall appears between the electrodes,²⁵ which mainly consists of $\text{Sn}(\text{OH})_2$ and $\text{Sn}(\text{OH})_4$.

For HASL, there are also lead hydroxide generation reactions between the electrodes:



Similarly, for Cu surface finish, when ions migrate between the electrodes due to electric field and concentration

gradient, and when the concentration requirements for the precipitation reaction are met, metal hydroxides are formed:



However, since the solubility product constant of $\text{Cu}(\text{OH})_2$ is 2.2×10^{-20} , the relatively large solubility product leads to its generation requiring high Cu^{2+} and OH^- concentration. Meanwhile, the generation of dendrites consumes a large amount of Cu^{2+} , resulting in the Cu^{2+} in solution remaining at a low level, so it is difficult to see the light-blue copper hydroxide $\text{Cu}(\text{OH})_2$ during the experiment.

As can be seen from Table II above, the standard electrode potential of tin is low, which means that tin metal is extremely easy to dissolve and generate tin ions in the presence of an applied electric field, and the small solubility products of $\text{Sn}(\text{OH})_2$ and $\text{Sn}(\text{OH})_4$ result in easier formation of these hydroxides, even for lower concentrations of $\text{Sn}^{2+}/\text{Sn}^{4+}$, so that it is extremely easy for white precipitates to appear during the test (e.g., Fig. 7).

Furthermore, copper metal has the highest standard electrode potential, and thus the dissolution rate of copper metal is much lower than that of tin metal under the same conditions. However, the ECM test results at the same bias voltage revealed that the growth of copper dendrites was much more drastic than that of the lead-free HASL/HASL, which can be explained to some extent by the solubility product of $\text{Cu}(\text{OH})_2$: Although the dissolution rate of the Cu electrode was smaller than that of the tin electrodes at the same time, the larger solubility product of $\text{Cu}(\text{OH})_2$ resulted in its

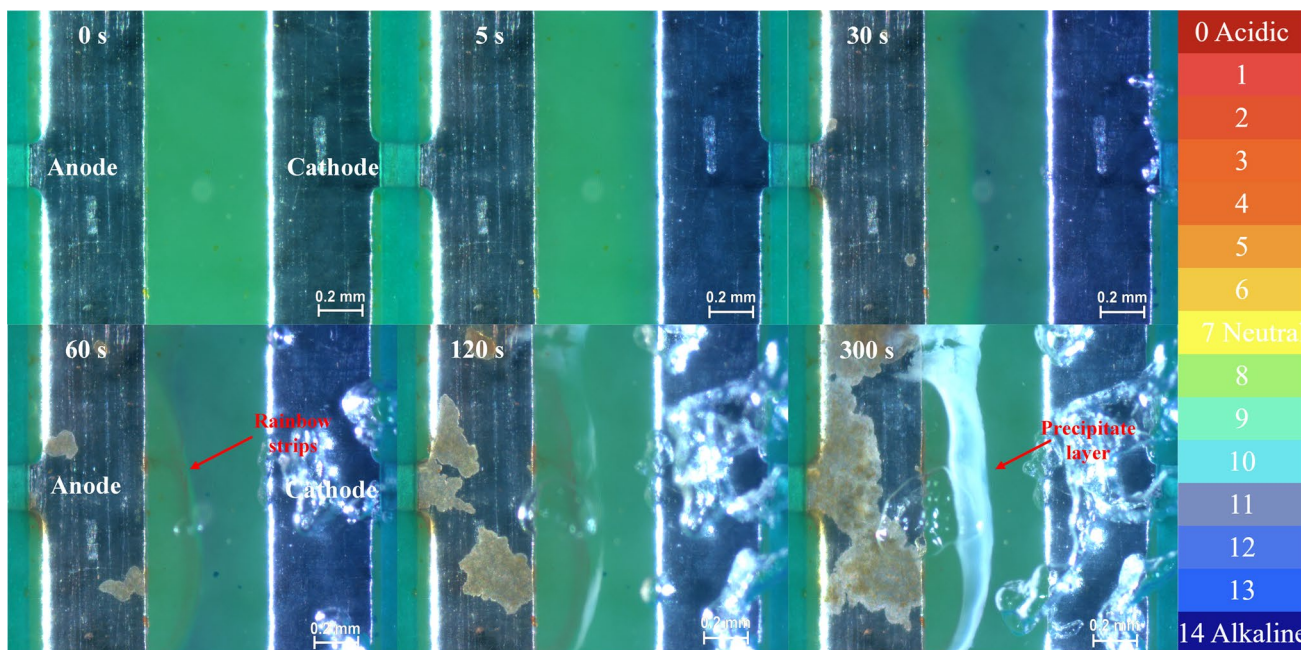


Fig. 8 Lead-free HASL sample at 3 V voltage bias (300 s).

Table II Metal standard electrode potential & hydroxide solubility product

Metal	Standard electrode potential	Metal hydroxide	Solubility	Color	References
Sn	−0.136 (Sn ²⁺)	Sn(OH) ₂	5.45 × 10 ^{−28}	White	26
		Sn(OH) ₄	1.0 × 10 ^{−56}	White	26
Pb	−0.126	Pb(OH) ₂	1.0 × 10 ^{−16}	White	27
Cu	0.340	Cu(OH) ₂	2.2 × 10 ^{−20}	Light-blue	27
Ni	−0.257	Ni(OH) ₂	2.0 × 10 ^{−15}	Green	28

generation requiring a higher Cu²⁺ and concentration. Therefore, the accumulative concentration of metal ions for Cu is higher than that of HASL(lead-free) during the test, resulting in the Cu surface finish being more prone to dendrite growth and failure due to the accumulation of free metal ions between the electrodes under the same conditions. This also indicates that the rate of dendrite growth is more correlated with metal ion hydroxide than with the standard electrode potential of the metal.¹⁹ Moreover, the solubility product of Pb(OH)₂ is much higher than that of Sn(OH)₂, Sn(OH)₄, and Cu(OH)₂, which leads to the presence of a large number of Pb²⁺ ions between the electrodes, so the critical current density for triggering dendrite growth can be easily exceeded. This is verified by the experimental results, which show that the occurrence of ECM failure for HASL is much less difficult than for lead-free HASL.

For the ENIG surface finish, despite the absence of ECM, the nature of the nickel metal, as shown in Table II, still yields a large amount of Ni metal dissolution, which takes place at the intermediate nickel layer in the ENIG structure. In the literature,²⁹ it has been reported that pure gold experiences ECM phenomena in deionized water at higher bias voltages. It was also concluded³⁰ that in the case of ENIG electrodes in double-distilled water, gold is detected as the main element of the dendrite, with the remaining elements comprising small amounts of nickel and copper, and no halogen contaminants detected. In another study,³¹ Ag was observed in the ECM of 96.5Sn-3Ag-0.5Cu alloy in NaCl solution and was potential-dependent. However, in our results, dendrites containing gold did not appear under all bias voltages, which can be explained as follows: Although it can be concluded by the standard electrode potential of gold (+1.498 V) that Au³⁺ ions are generated during the test, with no other pollutant such as chlorides affecting the process, the insoluble Au(OH)₃ is quickly generated on the anode surface, resulting in a low concentration of Au³⁺ ions between the electrodes. Also, due to the thick Ni layer (3–6 μm) of the ENIG surface finish, it is difficult for the solution to penetrate the Cu matrix and cause its dissolution. Finally, it was reported³¹ that Ag always co-existed with Sn and Cu after ECM experiments in NaCl electrolyte. Nevertheless, in this paper, the ENIG surface does not include Sn, and no

Cu was found after ECM experiments. Therefore, it can be deduced that Ag is able to participate in the ECM process when it co-exists with other metals and pollutants that boost Ag migration, where chloride ion plays a huge role. In summary, the ENIG surface finish mainly produces nickel metal hydroxides and oxides during the ECM experiment in deionized water, as shown by the black-green deposits between the electrodes of ENIG in Fig. 3, which is consistent with the EDS observation.

Conclusions

In this study, the electrochemical migration behavior of typical PCB electrode surface finishes in deionized water was evaluated by a modified water drop test. The ECM failure was further analyzed by in situ observation and current monitoring between the electrodes. The ECM mechanism was investigated by surface morphology investigation and compositional analysis. The following conclusions were drawn:

- (1) For the lead-free HASL, HASL, and Cu surface finishes, dendritic products appeared during the experiments growing from the cathode to the anode, leading to local short circuits and surface insulation failure. The failed Cu test boards reached high short-circuit current of up to 15 mA at 10 V, which resulted from continuous dendrite connection. The time to failure for the test boards shortened with the increase of bias voltage, and all three surface finishes have different dendrite morphologies between the electrodes. The morphology of the dendrites differed between the three surface finishes, where the dendrites of the lead-free HASL surface finish have both tin-dominated and copper-dominated shapes.
- (2) The electrochemical migration process of ENIG differs from other surface finishes, with no dendrite growth. Only nickel hydroxide and oxide formed from the anode edge and migrated toward the cathode. Gold did not participate in the electrochemical migration process due to its low reaction rate and hindered migration without the interference of other pollutants. At 10 V bias voltage, the current between the electrodes did

not exceed 0.05 mA. No ENIG test board failure was observed in the experiment.

- (3) Analysis of the electrochemical migration mechanism of different surface finishes revealed that the growth of dendrite is mainly related to the hydroxide solubility product of metal ions. A smaller solubility product leads to the generation of a large amount of precipitation, which further hinders the emergence and growth of dendrites. For the ENIG surface finish, the gold is not involved in the electrochemical migration process and no typical cathodic dendrite growth mechanism exists for nickel, only the generation of hydroxide and oxide between the electrodes with low conductivity, which makes ENIG resistant to electrochemical migration. The resistance to electrochemical migration for all four surface finishes are in order: ENIG > lead-free HASL > HASL > Cu.

Acknowledgments This work is supported by the Fundamental Research Funds for the Central Universities of the Civil Aviation University of China (Grant No. 3122023017).

Author Contributions All authors contributed to the study conception and design. Conceptualization, methodology, and investigation were performed by XS and KW. The first draft of the manuscript was written by KW and XS. All authors commented on the several versions of manuscript. Visualization and data curation were performed by ZC. Formal analysis, reviewing and editing were done by KW. Supervision, funding acquisition and resources were provided by KR and PL.

Data Availability The authors confirm that the data supporting the findings of this study are available within the article.

Conflict of interest The authors declare that they have no known competing financial interests or personal relationships that could have appeared to influence the work reported in this paper.

References

- X.F. He, M.H. Azarian, and M.G. Pecht, Evaluation of electrochemical migration on printed circuit boards with lead-free and tin-lead solder. *J. Electron. Mater.* 40, 1921 (2011).
- B.K. Liao, H. Wang, S. Wan, W.P. Xiao, and X.P. Guo, Electrochemical migration inhibition of tin by disodium hydrogen phosphate in water drop test. *Metals* 10, 12 (2020).
- K. Piotrowska, M. Grzelak, and R. Ambat, No-Clean solder flux chemistry and temperature effects on humidity-related reliability of electronics. *J. Electron. Mater.* 48, 1207 (2019).
- M.S. Jellesen, D. Minzari, U. Rathinavelu, P. Moller, and R. Ambat, Corrosion failure due to flux residues in an electronic add-on device. *Eng. Fail. Anal.* 17, 1263 (2010).
- K. Dusek, D. Busek, P. Vesely, M. Placek, T. Reichl, and J. Sedlacek, Analysis of a failure in a molded package caused by electrochemical migration. *Eng. Fail. Anal.* 121, 105 (2021).
- H. Conseil-Gudla, F. Li, and R. Ambat, Reflow residues on printed circuit board assemblies and interaction with humidity. *IEEE Trans. Device Mater. Reliab.* 21, 594 (2021).
- X. Zhong, In situ study of the electrochemical migration of tin in the presence of H₂S. *J. Mater. Sci. Mater. Electron.* 31, 8996 (2020).
- E.L. Lee, A. Haseeb, W.J. Basirun, Y.H. Wong, M.F.M. Sabri, and B.Y. Low, In-situ study of electrochemical migration of tin in the presence of bromide ion. *Sci Rep.* 11, 15 (2021).
- S.Y. Jiang, B.K. Liao, Z.Y. Chen, and X.P. Guo, Investigation of electrochemical migration of tin and tin-based lead-free solder alloys under chloride-containing thin electrolyte layers. *Int. J. Electrochem. Sci.* 13, 9942 (2018).
- O.N. Kamil, O.F. Rifdi, and A.F. Che, Electrochemical migration and corrosion behaviours of SAC305 reinforced by NiO, Fe₂O₃, TiO₂ nanoparticles in NaCl solution. *IOP Conf. Ser. Mater. Sci. Eng.* 701, 012 (2019).
- B.K. Liao, H. Wang, L. Kang, S. Wan, X.D. Quan, and X.K. Zhong, Electrochemical migration behavior of low-temperature-sintered Ag nanoparticle paste using water-drop method. *J. Mater. Sci. Mater. Electron.* 32, 5680 (2021).
- G.Q. Lu, C.Y. Yan, Y.H. Mei, and X. Li, Dependence of electrochemical migration of sintered nanosilver on chloride. *Mater. Chem. Phys.* 151, 18 (2015).
- M.S. Hong, and J.G. Kim, Method for mitigating electrochemical migration on printed circuit boards. *J. Electron. Mater.* 48, 5012 (2019).
- H.L. Huang, X.M. Guo, F.R. Bu, and G.L. Huang, Corrosion behavior of immersion silver printed circuit board copper under a thin electrolyte layer. *Eng. Fail. Anal.* 117, 14 (2020).
- P. Yi, K. Xiao, C.F. Dong, S.W. Zou, and X.G. Li, Effects of mould on electrochemical migration behaviour of immersion silver finished printed circuit board. *Bioelectrochemistry* 119, 203 (2017).
- K. Xiao, P. Yi, C.F. Dong, S.W. Zou, and X.G. Li, Role of mold in electrochemical migration of copper-clad laminate and electroless nickel/immersion gold printed circuit boards. *Mater. Lett.* 210, 283 (2018).
- P. Yi, K. Xiao, K.K. Ding, C.F. Dong, and X.G. Li, Electrochemical migration behavior of copper-clad laminate and electroless nickel/immersion gold printed circuit boards under thin electrolyte layers. *Materials* 10, 137 (2018).
- S.W. Zou, X.G. Li, C.F. Dong, K.K. Ding, and K. Xiao, Electrochemical migration, whisker formation, and corrosion behavior of printed circuit board under wet H₂S environment. *Electrochim. Acta* 114, 363 (2013).
- B.I. Noh, J.W. Yoon, W.S. Hong, and S.B. Jung, Evaluation of electrochemical migration on flexible printed circuit boards with different surface finishes. *J. Electron. Mater.* 38, 902 (2019).
- W.S. Hong, and C. Oh, Lifetime prediction of electrochemical ion migration with various surface finishes of printed circuit boards. *J. Electron. Mater.* 49, 48 (2020).
- D. Bušek, K. Dušek, J. Kulhavý, Dendritic growth and its dependence on various conditions. 2018 41st International Spring Seminar on Electronics Technology (ISSE). 1 (2018).
- B. Medgyes, B. Illés, and G. Harsányi, Electrochemical migration behaviour of Cu, Sn, Ag and Sn63/Pb37. *J. Mater. Sci. Mater. Electron.* 23, 551–556 (2012).
- B. Illés, B. Medgyes, A. Horvath, IEEE. Electrochemical migration behaviour of surface finishes after vapour phase reflow soldering. Proceedings of the 20th IEEE International Symposium on Design and Technology in Electronic Packaging (SIITME). 253 (2014).
- S. Bahrebar, and R. Ambat, Investigation of critical factors effect to predict leakage current and time to failure due to ECM on PCB under humidity. *Microelectron Reliab.* 127, 14 (2021).
- X. Qi, H.R. Ma, C. Wang, S.Y. Shang, X.G. Li, and Y.P. Wang, Electrochemical migration behavior of Sn-based lead-free solder. *J. Mater. Sci. Mater. Electron.* 30, 695 (2019).

26. X.K. Zhong, L.J. Chen, B. Medgyes, Z. Zhang, S.J. Gao, and L. Jakab, Electrochemical migration of Sn and Sn solder alloys: a review. *RSC Adv.* 7, 186 (2017).
27. D. Dobos, *Electrochemical Data, A Handbook for Electrochemists in Industry and Universities* (Amsterdam: Elsevier Scientific, 1975).
28. S.V. Mattigod, D. Rai, A.R. Felmy, and L. Rao, Solubility and solubility product of crystalline Ni(OH)₂. *J. Solution Chem.* 26, 391 (1997).
29. P. Singh, M. Sunder, E. E. Campbell, L. Palmer. A case study of nickel dendritic growth on printed-circuit boards. 2020 Pan Pacific Microelectronics Symposium (Pan Pacific). 1 (2020).
30. B. Medgyes, A. Gharaibeh, D. Rigler, and G. Harsanyi, On the electrochemical migration mechanism of gold in electronics-less reliable than expected? *Materials* 14, 9 (2021).
31. X. Zhong, W. Lu, B. Liao, B. Medgyes, J. Hu, and Y. Zheng, Evidence for Ag participating the electrochemical migration of 96.5Sn-3Ag-0.5Cu alloy. *Corros. Sci.* 156, 10 (2019).

Publisher's Note Springer Nature remains neutral with regard to jurisdictional claims in published maps and institutional affiliations.

Springer Nature or its licensor (e.g. a society or other partner) holds exclusive rights to this article under a publishing agreement with the author(s) or other rightsholder(s); author self-archiving of the accepted manuscript version of this article is solely governed by the terms of such publishing agreement and applicable law.